Vol. 22, No. 2(2023) Ener2320
Revista Mexicana de Ingeniería Química

Bioelectrochemical behavior of Ordered Mesoporous Carbon + *B. subtilis* as bioanode for the production of bioenergy in a Microbial Fuel Cell (MFC)

Comportamiento bioelectroquímico de Carbón Mesoporoso Ordenado + *B. subtilis* como bioánodo para la producción de bioenergía en una Celda de Combustible Microbiana (CCM)

S. García-Mayagotia[1], F.J. Rodríguez-Varela[1]*, F. Fernández-Luqueño[1], C.R. Sarabia-Castillo[1], J.C. Carrillo-Rodríguez[1], I.L. Alonso-Lemus[2], P.C. Meléndez-González[3], B. Escobar-Morales[4]

[1]*Sustentabilidad de los Recursos Naturales y Energía, Cinvestav Unidad Saltillo, Av. Industria Metalúrgica 1062, Ramos Arizpe, Coahuila, México.*

[2]*CONAHCyT-Cinvestav Saltillo. Sustentabilidad de los Recursos Naturales y Energía. Av. Industria Metalúrgica 1062, Parque Industrial Ramos Arizpe. Ramos Arizpe, Coahuila, C.P 25900, México.*

[3]*Universidad Autónoma de Nuevo León, (UANL) Facultad de Ciencias Químicas, Ave. Universidad S/N, Cd. Universidad, San Nicolás de los Garza N.L. México, C.P. 66455.*

[4]*CONAHCyT, Centro de Investigación Científica de Yucatán, Unidad de Energía Renovable, Carretera Sierra Papacal-Chuburná Puerto, Km 5, Sierra Papacal, México*

Received: April 29, 2023; Accepted: June 26, 2023

Abstract

The bioelectrochemical behavior of non-functionalized Ordered Mesoporous Carbon (OMC) and functionalized with methanol at different concentrations (0.15, 0.5 and 1 M, labeled as OMC015, OMC05, and OMC1, respectively), forming bioanodes with *Bacillus subtilis* (*B. subtilis*) as the electrochemically active microorganism (EAM), was evaluated in a dual-chamber Microbial Fuel Cell (MFC). OMC015 showed the highest surface area (550.0 $m^2\ g^{-1}$) with a total pore volume of 0.270 $cm^3\ g^{-1}$ (those of OMC were 410.6 $m^2\ g^{-1}$ and 0.191 $cm^3\ g^{-1}$, respectively). Cyclic voltammograms (CVs) in pharmaceutical wastewater (PWW, pH= 7.1) showed an enhanced bioelectrochemical behavior of the OMC + *B. subtilis* and OMC015 + *B. subtilis* bioanodes compared to OMC05 + *B. subtilis* and OMC1 + *B. subtilis*. Therefore, the two former bioanodes were evaluated in the MFC containing PWW as substrate in the anode chamber. The results showed differences in the behavior of the bioanodes in long-term tests (7 days) in the MFC. OMC + *B. subtilis* showed a decrease in Open Circuit Voltage (OCV) and current density (j) values from Day 0 to Day 3, followed by a slight increase in j and a higher OCV at Day 7 (compared to Day 3). Meanwhile, OMC015 + *B. subtilis* showed a more stable bioelectrochemical behavior, with slight variations in OCV and j at Days 0, 3 and 7. The maximum power density (P_{cell}) of the MFC was 12.3 mW m^{-2} with OMC015 + *B. subtilis* at Day 3 of operation. The results showed the biocompatibility between the OMC015 catalysts and *B. subtilis* as EAM, and their catalytic activity to oxidize organic matter contained in PWW, generating bioenergy from the MFC.

Keywords: Ordered Mesoporous Carbon, *B. subtilis*, pharmaceutical wastewater, Microbial Fuel Cells, bioelectrochemical energy.

Resumen

El comportamiento bioelectroquímico del Carbón Mesoporoso Ordenado (OMC) sin funcionalizar, y funcionalizado con metanol a diferentes concentraciones (0.15, 0.5 y 1 M, identificados como OMC015, OMC05 y OMC1, respectivamente), formando bioánodos con *Bacillus subtilis* (*B. subtilis*) como microorganismo electroquímicamente activo (EAM), fue evaluado en una Celda de Combustible Microbiana (MFC) de doble cámara. OMC015 mostró el área superficial más alta (550.0 $m^2 g^{-1}$) con un volumen total de poro de 0.270 $cm^3\ g^{-1}$ (OMC tuvo 410.6 $m^2\ g^{-1}$ y 0.191 $cm^3\ g^{-1}$, respectivamente). Los voltamperogramas cíclicos (CVs) en agua residual farmacéutica (PWW, pH= 7.1) mostraron un mejor comportamiento bioelectroquímico de los bioánodos OMC + *B. subtilis* y OMC015 + *B. subtilis*, comparados con OMC05 + *B. subtilis* y OMC1 + *B. subtilis*. Por lo tanto, los dos primeros bioánodos fueron evaluados en la MFC conteniendo PWW como sustrato en la cámara del ánodo. Los resultados mostraron diferencias en el comportamiento de los bioánodos en pruebas de larga duración (7 días) en la MFC. OMC + *B. subtilis* mostró una disminución en los valores de voltaje de circuito abierto (OCV) y de densidad de corriente (j) del Día 0 al día 3, seguido de un incremento ligero en j y un OCV mayor en el Día 7 (comparado con el Día 3). Mientras tanto, OMC015 + *B. subtilis* tuvo un comportamiento bioelectroquímico más estable, con variaciones menores en OCV y j en los Días 0, 3 y 7. La densidad de potencia máxima (P_{cell}) de la MFC fue de 12.3 mW m^{-2} con OMC015 + *B. subtilis* en el Día 3 de operación. Los resultados mostraron la biocompatibilidad entre el catalizador OMC015 y *B. subtilis* como EAM, así como su actividad catalítica para oxidar la materia orgánica contenida en PWW, generando bioenergía de la MFC.

Palabras clave: Carbón Mesoporoso Ordenado, *B. subtilis*, agua residual farmacéutica, Celdas de Combustible Microbianas, energía bioelectroquímica.

*Corresponding author. *E-mail*: javier.varela@cinvestav.edu.mx
https://doi.org/10.24275/rmiq/Ener2320
ISSN:1665-2738, *issn-e*: 2395-8472

1 Introduction

Nowadays, fossil fuels such as oil, natural gas, and coal remain the most important energy sources worldwide (International Energy Agency, 2023). However, such fuels are not renewable, and their availability is becoming more limited every year. Moreover, their combustion in any application produces CO_2, SO_x, and NO_x, i.e., greenhouse gases (GHG), resulting in environmental pollution (Islam, *et al*., 2023). Over the past decade, research groups have searched for cleaner alternatives for energy generation. One of those is that of bioelectrochemical devices, such as MFCs, to produce bioenergy as a sustainable alternative to the use of fossil fuels (Zhou, *et al*., 2014); (Zhao, *et al*., 2022). MFCs can aerobically/anaerobically oxidize the organic matter contained in a substrate (i.e., PWW) to generate electrons in the bioanode, which are transported to the cathode via an external circuit. As a result, V and j values are produced between the bioanode and the cathode. The result is the generation of a P_{cell} (Conzuelo, *et al*., 218). Moreover, the oxidation of organic matter results in the treatment of the substrate (Rashid, *et al*., 2021).

B. subtilis has been identified as producer of β-lactamase enzymes, which degrades β-lactam compounds contained in PWW (Al-Gheethi, et al., 2019). This is highly relevant, since ampicillin, a photo-resistant β-lactam antibiotic commonly found in PWW, is highly difficult to remove using conventional wastewater treatments (Vidal, et al., 2019). Thus, *B. subtilis* is an EAM that can produce electrons from the oxidation of organic matter in PWW, promoting its treatment (Pant & Patil, 2022). On this issue, it has been reported recently that *B. subtilis* EL06 can remove sulfadiazine while producing energy in an MFC with ca. 90% efficiency (Al-Ansari, *et al*., 2021).

Nevertheless, chemical elements and anthropogenic wastes in PWW can adversely affect the overall performance of an MFC. Therefore, the application of noble metal-free carbon-based catalysts in bioanodes of MFCs has been investigated by the scientific community. This comes as no surprise, since active materials such as N-doped carbon obtained from pharmaceutical wastes have been used to electrochemically reduced CO_2 to CO (Gang, *et al*., 2023). Therefore, a catalyst layer deposited on a carbon cloth electrode in contact with the biofilm of the EAM enhances the electron transfer to the external circuit, thus improving the P_{cell} delivered by the MFC (García-Mayagoitia, *et al*., 2019). Carbon-based catalysts such as paper, cloth, mesh, reticulated vitreous, OMC, and biocarbons, have been successfully utilized in bioanodes of MFC (Kipf, *et al*., 2013; Morales-Acosta, *et al*., 2016; Plekhanova, *et al*., 2022).

It is acknowledged that several physicochemical characteristics of carbon catalysts are relevant to: i) improve the transport of species (surface area, average pore size, micro/mesoporosity, interconnected channels); and ii) to assure the growth and attachment of the biofilm developed by the EAM (surface functional groups, particularly oxygen-containing species). Enhanced characteristics of the carbon-based materials play a positive role promoting the biocompatibility of the catalyst layer/biofilm interface, and therefore the extracellular electron transfer (EET) (Cui, *et al*., 2014). From those characteristics, highly performant bioanodes are formed to produce energy and proceed with the treatment of the substrate (Kipf, *et al*., 2013; Szopińska, *et al*., 2023).

The novelty of this work is the study of the effect of functionalizing OMC with several concentrations of methanol on the development of surface functional groups, and therefore on its catalytic activity and biocompatibility with *B. subtilis*. Moreover, the pH of the PWW substrate is 7.1, compared to 9.6 in our previous report (García-Mayagoitia, *et al*., 2019), which may put to test the performance of the EAM in the 7-days testing, despite the high adaptation capacity of *B. subtilis* to survive in harsh media (Ryu, *et al*., 2022), i.e., the alkalinity of the substrate may affect the kinetics of the EET. Moreover, the innovation of this work is related to the development and application of the OMC + *B. subtilis* bioanodes for renewable energy generation from as received PWW, demonstrating the potential of MFC to replace conventional and polluting fossil-fuel based systems.

The bioelectrochemical behavior of bioanodes formed by a catalyst layer of non-functionalized and functionalized OMC and a biofilm of *B. subtilis* has been characterized in half-cell and MFC tests. The performance of the MFC is evaluated in terms of V-j and P_{cell}-j curves. Moreover, the behavior of the bioanodes is studied using electrochemical impedance spectroscopy (EIS).

2 Materials and methods

2.1 Synthesis and functionalization of OMC

OMC was synthesized via a two-step synthesis, already described in detail elsewhere (Morales-Acosta, *et al*., 2016). Briefly, resorcinol (8.81 g), formaldehyde (24.88 mL), and sodium carbonate (0.04 g, alkaline catalyst) were mixed by stirring for 1 h. After this pre-polymerization, a mixture containing Pluronic F127 triblock copolymer (6.2 g), deionized water (16 mL), and ethanol (25 mL) was added to the solution containing the carbon precursors, maintaining stirring for 1 h. The copolymer obtained was used as a template to promote the formation of the hexagonal mesostructure of the OMC. Afterwards, 8 mL of 2 M HCl were added to the solution, sustaining vigorous agitation for 1 h. The orange resin obtained was dried at 80°C for 24 h, and carbonized at 900°C in N_2 atmosphere for 3 h at a heat rate of 1°C per min. The resulting solid was pulverized in a Fritsch Pulverisette planetary mill for 10 min and sieved using a 100 mesh.

The intermittent microwave heating (IMH) process was implemented to functionalize OMC powders. The procedure was as follows: 2 g of OMC were separately sonicated in 200 mL of 0.15, 0.5, and 1 mol L^{-1} methanol (MeOH) solutions for 30 min, followed by magnetic stirring for 1 h. The mixtures were thermally treated in a microwave oven for 8 min applying pulses 25 s on/15 s off under stirring and refluxing conditions. The powders were filtered, washed, dried for 24 h, and calcined at 200ºC for 30 min. The functionalized OMC catalysts were labeled as OMC015, OMC05, and OMC1, respectively.

Table 1. Physicochemical properties of pharmaceutical wastewater used as substrate in the Microbial Fuel Cell, at the onset of the experiments.

Parameter	
pH	7.10
Specific conductance (mS cm^{-1})	29.22
Oxidation and reduction potential (mV)	53.40
Resistance (ohm cm^{-1})	52.79
Temperature (°C)	23.37
Chemical oxygen demand (mg L^{-1})	14191.51

2.2 Microorganism and anode substrate

The microbial strain *B. subtilis* (CDBB 1349) was provided by the National Collection of Microbial Strains and Cell Cultures of Cinvestav. The strain was activated in Petri dishes containing 10 mL of LB nutritive agar and incubated for 72 h at 28°C in a Vichi INO Incubator. The inoculum, i.e., the culture media containing grown bacteria, was adjusted into 5 mL tubes and placed in a freezer at -20°C for its later use for the growth of biofilms.

The PWW used as anode substrate was obtained from a pharmaceutical company located in Ramos Arizpe, Coahuila, México. The PWW was collected following the composite sample technique: every 30 min, 1 L plastic bottles were filled out at the effluent of the factory, reaching a total volume of 14 L that were mixed homogeneously and transported in a cooler to avoid altering its composition. Afterwards, it was stored at -20ºC to avoid microbial growth contamination until its use in the MFC. Table 1 shows the physicochemical properties of the PWW. As can be observed, the properties changed considerably from those reports previously by our group of a similar PWW (García-Mayagoitia, *et al*., 2019). For example, the pH in this study was determined as 7.1, while previously it was 9.6.

2.3 Physicochemical characterization

X-Ray Diffraction (XRD) patterns were obtained in an Empyrean PANalytical equipment in the 10-100° (2θ) interval. Chemical composition was determined using a Phillips X'Pert Scanning Electron Microscope (SEM) equipped with an Energy Dispersive Spectroscopy (EDS) detector operating at an accelerating voltage of 20 kV. Fourier Transform Infrared spectra (FT-IR) were acquired using a Bruker Tensor II spectrometer in the 4000-500 cm^{-1} range using the ATR technique. Raman spectra were acquired in a DXR2 Thermo Scientific model at a wavelength of 633 nm in the 100 to 3500 cm^{-1} range.

Morphology analysis and chemical mapping were performed in a Jeol 7800 F Field Emission Scanning Electron Microscope (FESEM). High Resolution Transmission Electron Microscopy (HRTEM) analysis was performed using a Talos 200 FEI equipment at an accelerating voltage of 200 kV. Textural properties were analyzed by N_2 adsorption/desorption by applying a BET analysis in a Quantachrome Autosorb Automated Gas Sorption System. Surface chemical compositions were determined by X-ray Photoelectron Spectrometry (XPS) using a K-Alpha Thermo Scientific spectrometer with a monochromatic Al Kα X-ray source (1486.68 eV). Spectra were charge compensated by using binding energy (BE) of 284.8 eV of the C 1s region of adventitious carbon.

2.4 Fabrication of anodes, bioanodes and cathodes

ELAT LT-1200 W carbon cloths (BASF) were used for the fabrication of the electrodes. Catalyst inks were separately prepared by ultrasonically mixing for 30 min powders of OMC, OMC015, OMC05 and OMC1 with Nafion® solution (5 wt. %, Sigma Aldrich) and 2-propanol (J.T. Baker) in a 3.5:1:1 wt. % ratio (Rodríguez-Varela & Savadogo, 2009). For the manufacturing of anodes, a catalyst layer of each carbon material was deposited over carbon cloths of 1 cm^2 geometric area using a micropipette, achieving a catalyst loading of 5 mg cm^{-2}.

The bioanodes were obtained after placing the corresponding anodes in 100 mL of LB liquid media inoculated with *B. subtilis*, allowing the biofilm to grow for 6 days in a Vichi INO incubator at 28°C. The cathodes were fabricated by depositing using the same technique 2 mg cm^{-1} catalyst layers of commercial 20 wt. % Pt/C on 1 cm^2 geometric area carbon cloths.

2.4.1 Physicochemical characterization of bioanodes

The morphology of the bioanodes was characterized by SEM in an XL30 Philips microscope at 10 kV accelerating voltage. After biofilm growth, samples of bioanodes were submerged in Trump´s solution (4 mL of 25% grade I glutaraldehyde, 10 mL of 37% formaldehyde, and 0.27 g of sodium hydroxide, diluted to 100 mL with bi-distilled water) and refrigerated for 24 h. Afterwards, the bioanodes were dehydrated by sequentially placing them in 40, 50, 60, 70, 80, 90, and 100% ethanol solutions for 30 min each, and left to dry in a desiccator for 24 h.

2.5 Electrochemical characterization

2.5.1 Half-cell

The catalytic activity of anodes and bioanodes was characterized in an electrochemical three-electrode half-cell. An Ag/AgCl (in saturated 3 M NaCl) and a graphite rod acted as reference and counter electrode, respectively. Meanwhile, the working electrode consisted of the anodes and bioanodes described above. An electrical contact was promoted by fixing copper wire to the opposite face of the electrodes containing the catalyst layer using carbon catalytic ink. The electrodes were covered with epoxy resin, limiting the active geometric area to 1 cm^2.

The electrochemical behavior of anodes and bioanodes was evaluated by cyclic voltammetry in PWW as substrate, with a BioLogic SAS VSP-300 bipotentiostat. Cyclic voltammograms (CVs) were acquired in the 50-1200 mV potential interval in the Reversible Hydrogen Electrode (RHE). Conversion from the Ag/AgCl to the RHE scale was made with the Nernst equation as shown elsewhere (Alonso-Lemus, et al., 2022).

2.5.2 *Dual-chamber Microbial Fuel Cell*

2.5.2.1. Electrochemical Impedance Spectroscopy (EIS)

Nyquist plots of the OMC + *B. subtilis* and OMC015 + *B. subtilis* bioanodes as working electrodes were obtained in a frequency range between 10 kHz and 1 mHz, with an amplitude of 10 mV at Day 0, before obtaining the polarization curves described in the following section. The Ag/AgCl reference electrode was placed in the anode chamber, while the Pt/C electrode in the cathode chamber was used as the counter electrode (He & Mansfeld, 2009). A Randles equivalent circuit was used to fit the experimental results with the EC Lab software.

2.5.2.2. V-j and P_{cell}-j polarization curves

The MFC consisted of anode and cathode chambers separated by a Nafion 117 membrane (ION Power Inc.), previously activated with neutralizing reactions utilizing H_2O_2 and H_2SO_4, removing residues with boiling deionized water (Rodríguez-Varela & Savadogo, 2009). The cathode chamber contained the Pt/C electrode in O_2-saturated phosphate buffer solution, while PWW was adjusted to the anode chamber as substrate under continuous magnetic stirring, with the bioanodes submerged within. The MFC operated at room temperature. The bioanodes evaluated were OMC + *B. subtilis* and OMC015 + *B. subtilis* (Figure S1).

For the characterization of the MFC, cell voltage (E_{cell}) vs. j polarization curves were obtained using the bipotentiostat and a set of external resistances. First, the open circuit voltage (OCV) of the cell was measured. Then, external resistances (R_{ext}) of 0.0071, 1.21, 5, and 10 kΩ were imposed to measure E_{cell} and from such values, the cell current (I_{cell}) from Ohm's law (eq. 2) was determined. The j values were obtained by normalizing I_{cell} by the geometric area of the electrodes (A_{geo}), as shown in eq. (3). Meanwhile, P_{cell} was obtained with eq. (4):

$$I_{cell} = \frac{E_{cell}}{R_{ext}} \quad (1)$$

$$j = \frac{I_{cell}}{A_{geo}} \quad (2)$$

$$P_{cell} = E_{cell} j \quad (3)$$

During the long-term tests, the MFC was polarized by applying R_{ext}= 10 kΩ.

3 Results and discussions

3.1 *Physicochemical characterization of the OMC catalysts*

Figure 1 depicts the XRD patterns of OMC, OMC015, OMC05, and OMC1. The catalysts show reflections at 22.5 and 43.6° (2θ), attributed to the (002) and (100) carbon planes (JCPDS 41-1487), characteristic of graphitic structures. The broad feature of the peaks indicates the amorphous nature of the OMC catalysts (Ma, *et al*., 2019). No significant differences can be observed between non-functionalized and functionalized OMC.

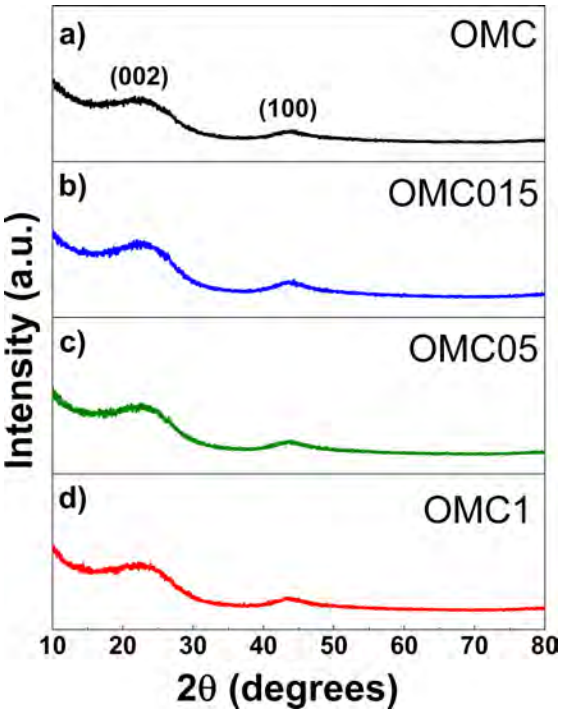

Figure 1. XRD patterns of a) OMC, b) OMC015, c) OMC05, and d) OMC1.

The chemical composition and standard deviation of non-functionalized and functionalized OMC is shown in Table S1. The concentration of C and O at OMC is ca. 98.78 and 1.22 (wt. %), respectively. The IMH affects the chemical composition of the catalysts, because of the presence of MeOH during treatment and due to the fact that carbon materials are sensitive to microwave radiation (Bharti & Cheruvally, 2017). With 0.15 M MeOH, the main influence is on the O content at the OMC015 catalyst since its concentration decreases. It is likely that the microwave heat treatment in the relatively low MeOH concentration causes removal of residual oxygen-containing species. At higher MeOH concentrations, the C content decreases at OMC05 and OMC1, reaching a minimum at the former. Conversely, the O content increases to 7.03 (wt. %) at OMC05 with a slight decrease at OMC1, apparently because of a surface saturation with oxygen-like species at higher MeOH concentrations.

Figure 2 shows the Raman spectra of non-functionalized and functionalized OMC. The D (associated with structural disorder or defects, at ca. 1320 cm^{-1}) and G (attributed to structural order or sp^2 carbon hybridization, at ~1580 cm^{-1}) bands, typical of carbon-based materials, are observed (Ma, Yuan, & Hu, 2019). The ratio of the intensities between the D and G bands (I_D/I_G) of OMC is 1.08, decreasing to 1.03 after functionalization with 0.15 M MeOH. The results indicate that microwave heating with a low MeOH concentration slightly increases the graphitic structural order i.e., a more intense G band of OMC015 than non-functionalized OMC. Meanwhile, the opposite occurs at OMC05 and OMC1, at which a higher MeOH concentration during IMH provokes an increase in their ID/IG ratio (1.16 and 1.46, respectively), compared to OMC and OMC015.

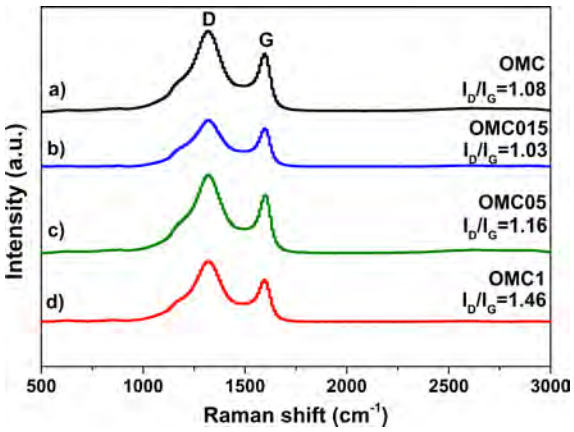

Figure 2. Raman spectra of a) OMC, b) OMC015, c) OMC05, and d) OMC1.

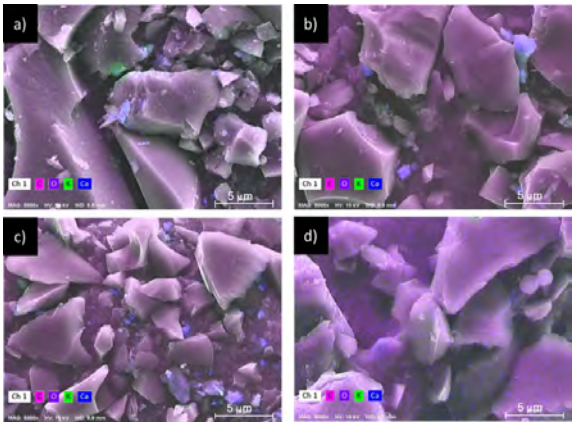

Figure 3. FESEM micrographs and chemical mapping of a) OMC, b) OMC015, c) OMC05, and d) OMC1.

The FTIR spectra of OMC, OMC015, OMC05, and OMC1 are shown in Figure S2. The non-functionalized catalyst shows low intensity bands at 3773 and 3718 cm^{-1} ascribed to ν(O-H) stretching vibrations, and relatively more intense signals at 1629 cm^{-1} due to C=C vibrations of carbonyl groups (Lian, et al., 2019). While OMC015 shows the same bands, it calls the attention that the relative intensity of the ν(O-H) and C=C bonds increases compared to OMC. Meanwhile, the relative intensity of the ν(O-H) vibrations at OMC05 and OMC1 is higher than that of OMC015. Such feature is ascribed to the IMH functionalization with higher MeOH concentrations, promoting the formation of O-H functional groups. On the other hand, it should be mentioned that the relative intensity of the C=C signal is lower at OMC05 and not clearly detected at OMC1, compared to OMC015.

The morphology and chemical mapping of the OMC catalysts are shown in Figure 3. The micrographs show a rather similar morphology, with large particles of irregular shape. As already mentioned in the SEM-EDS analysis, the most abundant elements at the catalysts are C and O, although with the FESEM technique traces of K and Ca have been detected. This morphology is expected based on previous studies on similar OMC materials (Lilloja, *et al*., 2023). The functionalization with MeOH, a soft chemical agent, has no effect on the morphology of the carbon-based catalysts. Figure S3 shows a HRTEM micrograph of OMC, at which the ordered arrangement of lattice fringes corresponding to its graphitized structure (e.g., the area highlighted by a red square) can be distinguished. This feature has been ascribed to the partial crystallinity of OMC (García-Mayagoitia, *et al*., 2019).

The N_2 adsorption-desorption isotherms of the OMC catalysts are shown in Figure 4. All isotherms have open hysteresis at low P/P0. The open characteristic is typical of slit or bottle-shaped pores, at which the adsorbate penetration is kinetically slow due the narrowness of the intrachannels of the carbon materials (Ma, Yuan, & Hu, 2019; Maziarka, *et al*., 2021). The isotherms fall in the type IVa classification (Thommes, *et al*., 2015; Kan, *et al*., 2023). Moreover, the materials show a steep increase in adsorption at high P/P0 while a hysteresis loop appears as a typical feature of micro-mesoporous structures (Ma, *et al*., 2019).

It can be seen in Table 2 that the surface area increases from 410.6 at OMC to 550 m^2 g^{-1} at OMC015 after functionalization with 0.15 M MeOH. The average pore size (reaching ca. 2 nm) and the total pore volume also become higher at the latter (0.270 vs. 0.191 cm^3 g^{-1}, respectively). The microwave radiation falls between the infrared and the radiowaves (ca. 10^{-3} to 1 m, (Menéndez, *et al*., 2010). It has been reported that carbon materials are active to microwave radiation (Bharti & Cheruvally, 2017). It is hypothesized that exposure of OMC to microwave radiation in 0.15 M MeOH removes some impurities, which can be correlated with the chemical composition in Table S1. The results show that OMC and OMC015 have a C content of ca. 98.78 and 99.89 wt. %, respectively, with less O at the latter. A slightly similar tendency can be seen in Table S2. Simultaneously, the relatively diluted MeOH solution can impregnate available pores, increasing their volume under intermittent heating, therefore producing a higher surface area at OMC015.

At OMC05 and OMC1, a contrary effect is observed compared to OMC015, i.e., their content of C and O decreases and increases, respectively, compared to OMC. Apparently, the relatively higher MeOH concentration inhibits the removal of impurities, avoids the activation of pores, or even provokes a collapse of a number of them under radiation, thus limiting the surface area. Even though more studies, out of the scope of this work, may be needed to determine an optimal MeOH concentration to generate a higher surface area, it seems that lower concentrations promote enhanced textural properties of OMC. Overall, the average pore size of the OMC catalysts falls within the micro-mesoporosity limit.

Table S2 depicts the surface chemical composition from the XPS survey of the OMC catalysts, composed mainly of C and O, with traces of Na at the non-functionalized catalyst because of the precursor used in the synthesis process, which is not detected after functionalization. There is an increase in the relative concentration of surface C after functionalization, with a slight decrease in that of O.

In Figure 5, the high-resolution XPS spectra of the OMC catalysts in the C 1s region can be observed. It depicts characteristic peaks ascribed to C=C sp^2, C-C sp^3, C-OH, C=O, and O-C=O species (Weidenthaler, *et al*., 2006; Wang, *et al*., 2020; Carrillo-Rodríguez, *et al*., 2021; Pérez-

Rodríguez, *et al*., 2019), The relative atomic concentration and the binding energy (BE) of the species are shown in Table 3. As can be observed, the highest concentration (roughly 80 at. %) is that of the sp^2 nanodomains (at ca. 284 eV) in the four OMC catalysts.

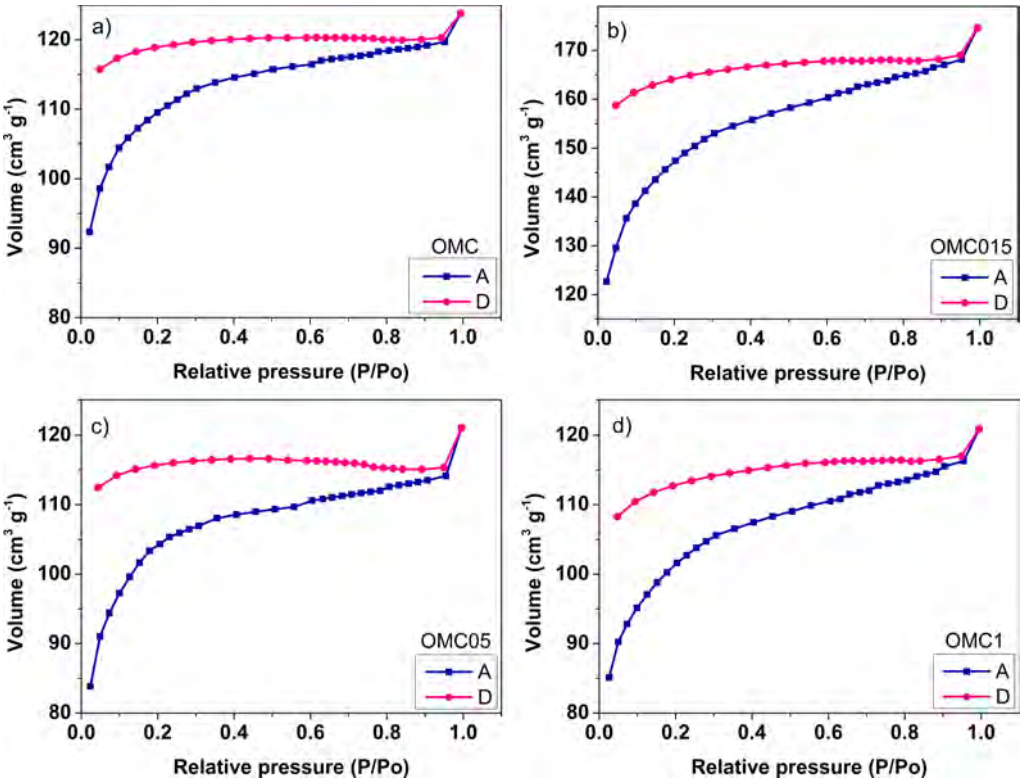

Figure 4. N_2 adsorption (A)-desorption (D) isotherms of a) OMC, b) OMC015, c) OMC05, and d) OMC1.

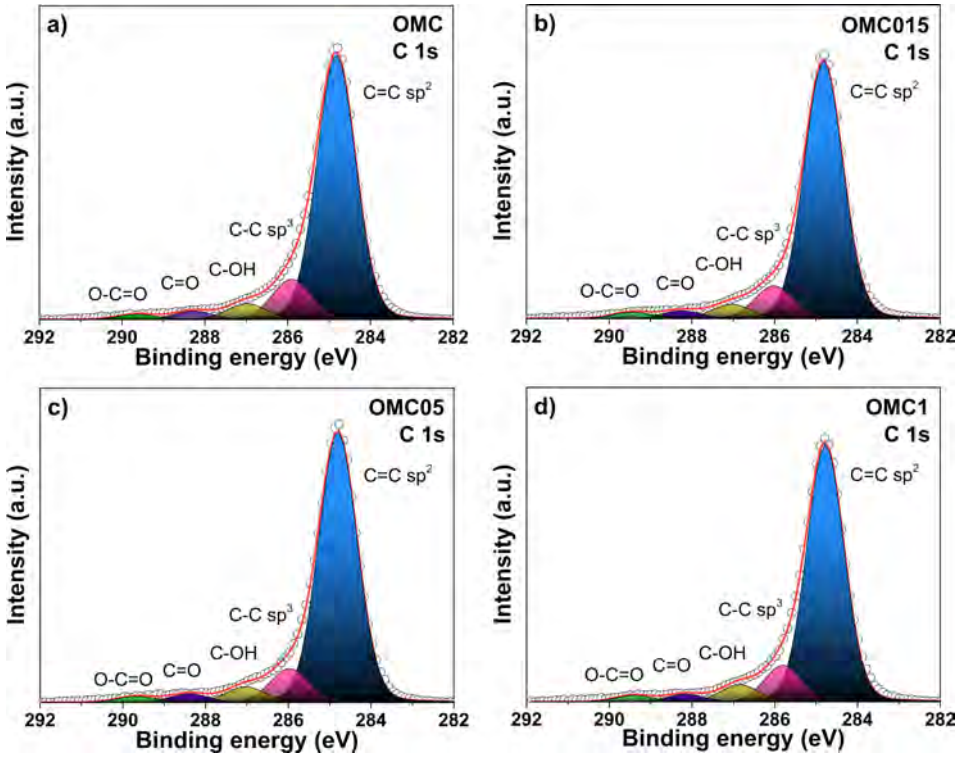

Figure 5. High resolution spectra in the C 1s region of OMC, OMC015, OMC05, and OMC1.

Table 2. Textural properties of OMC, OMC015, OMC05, and OMC1.

Sample	Surface area (m^2 g^{-1})	Average pore size (nm)	Total pore volume (cm^3 g^{-1})
OMC	410.6	1.865	0.191
OMC015	550	1.964	0.27
OMC05	380.1	1.971	0.187
OMC1	382	1.958	0.187

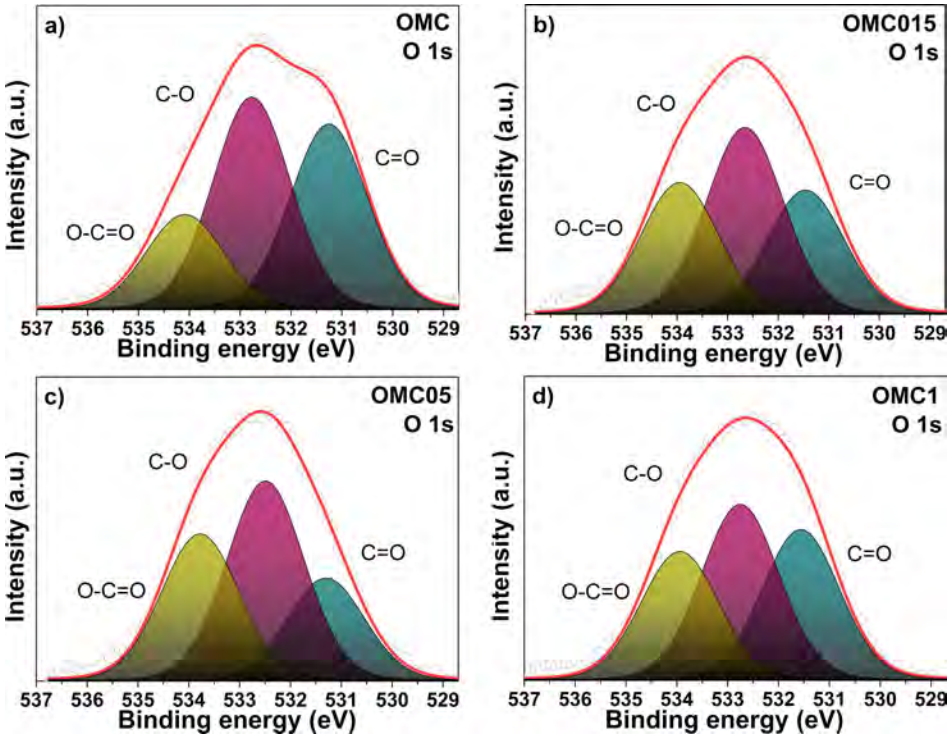

Figure 6. High resolution spectra in the O 1s region of OMC, OMC015, OMC05, and OMC1.

Table 3. High-resolution XPS data of the OMC catalysts.

Catalyst	Species	State	BE (eV)	Composition (at. %)
OMC	C=C sp^2	C 1s	284.82	79.1
	C-C sp^3	C 1s	285.91	12
	C-OH	C 1s	286.99	4.8
	C=O	C 1s	288.27	2.5
	O-C=O	C 1s	289.62	1.6
	C=O	O 1s	531.26	37.6
	C-O	O 1s	532.77	43.1
	O-C=O	O 1s	534.09	19.3
OMC015	C=C sp^2	C 1s	284.82	80.7
	C-C sp^3	C 1s	286.01	10.3
	C-OH	C 1s	287.04	4.5
	C=O	C 1s	288.25	2.5
	O-C=O	C 1s	289.45	2
	C=O	O 1s	531.46	28.1
	C-O	O 1s	532.66	42.1
	O-C=O	O 1s	533.95	29.8
OMC05	C=C sp^2	C 1s	284.8	80.7
	C-C sp^3	C 1s	285.98	10.2
	C-OH	C 1s	287.04	4.7
	C=O	C 1s	288.4	2.6
	O-C=O	C 1s	289.67	1.8
	C=O	O 1s	531.3	22.9

	C-O	O 1s	532.49	44.4
	O-C=O	O 1s	533.78	32.7
OMC1	C=C sp^2	C 1s	284.78	79.1
	C-C sp^3	C 1s	285.8	11.3
	C-OH	C 1s	286.86	5.3
	C=O	C 1s	288.15	2.3
	O-C=O	C 1s	289.4	2
	C=O	O 1s	531.56	33.1
	C-O	O 1s	532.75	38.6
	O-C=O	O 1s	533.94	28.3

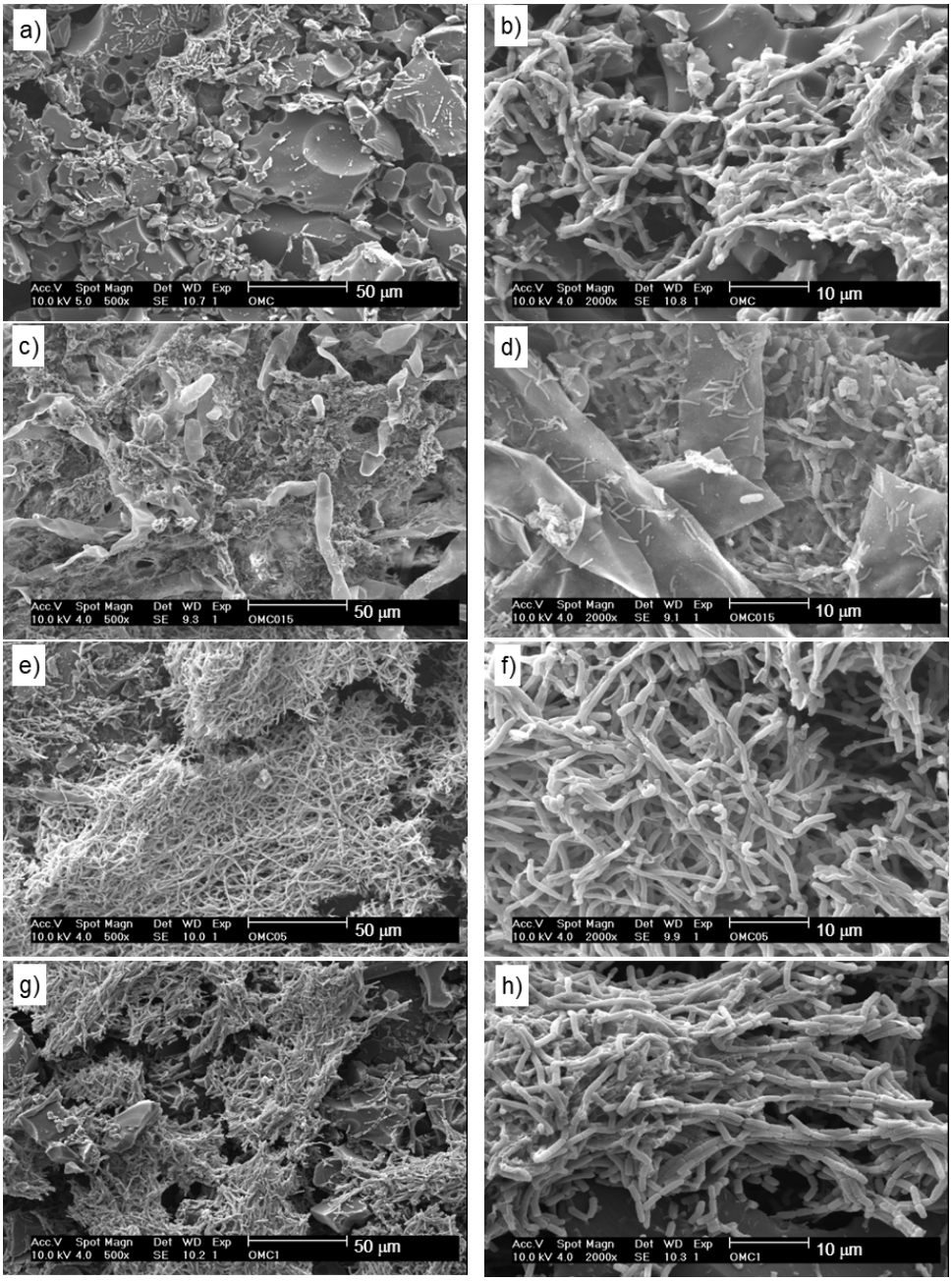

Figure 7. SEM micrographs of the bioanodes: a-b) OMC + *B. subtilis*, c-d) OMC015 + *B. subtilis*, e-f) OMC05 + *B. subtilis*, and g-h) OMC1 + *B. subtilis*.

Meanwhile, the high-resolution spectra in the O 1s region (Figure 6) shows the presence of the C=O, C-O, and O-C=O species (Wan, *et al*., 2020). Table 3 shows the relative atomic concentration of the species, the higher corresponding to the C-O species (BE about 532 eV). Overall, the C and O bonds in Figures 5 and 6 correspond to those normally observed elsewhere for carbon-based catalysts.

3.2 *Morphology of the bioanodes*

Figure 7 shows SEM micrographs of the bioanodes formed by the OMC catalysts and a biofilm by *B. subtilis* at two magnifications. The non-functionalized (Figure 7 a-b) and functionalized (Figures 7 c-h) bioanodes show a high degree of coverage by the biofilm over the carbonaceous catalysts, as confirmed by the well-developed extracellular matrix with rod-like shape bacteria. The formation of the biofilm can be attributed in part to the highly hydrophilic nature of the carbon surface, resulting in a carbon/EAM interface that suggests biocompatibility between the OMC catalysts and *B. subtilis*, (Xiao, *et al*., 2020) a fundamental feature to promote the electron transfer at the bioanodes (Patel, *et al*., 2019).

3.3 *Electrochemical behavior of the OMC + B. subtilis bioanodes*

Figure S4 displays the CVs of the non-functionalized and functionalized OMC anodes (i.e., without biofilm of *B. subtilis*) in N2-saturated PWW. OMC015, OMC05, and OMC1 generate higher j values at the most negative and positive potentials than OMC. Among the functionalized catalysts, OMC015 shows a slightly enhanced performance compared to OMC05 in terms of higher j, followed by OMC1. Thus, initially the functionalization with a relatively low concentration of MeOH has a positive effect on the electrochemical behavior of OMC, but a gradual increase in alcohol content during IMH hinders the generation of j. This behavior may be related to the development of OH-functional groups at the active surface of the functionalized OMC catalysts, as shown in Figure S2.

Figure 8 shows a comparison of the bioelectrochemical behavior of the anodes depicted in Figure S4 and the corresponding bioanodes: a) OMC + *B. subtilis*, b) OMC015 + *B. subtilis*, c) OMC05 + *B. subtilis*, and d) OMC1 + *B. subtilis*. It is seen that the presence of the EAM at the OMC + *B. subtilis* bioanode increases the j values at the more positive and negative potentials. As a consequence, the slope of its CV changes compared to the OMC anode, indicating an enhancement in biocatalytic activity at the carbon/EAM interface, thus improving the oxidation of organic matter from PWW and the EET at the bioanode (Modestra & Mohan, 2014; Duarte-Urbina, *et al*., 2021). Such behavior can be correlated to the coverage of the catalyst layer by the biofilm, as seen in Figures 7 a-b).

Similarly, the CV of OMC015 + *B. subtilis* shows a change in slope due to the generation of higher j values at the most positive potential, compared to OMC015 without EAM. Nevertheless, j at the more negative potentials is about the same at both bioanode and anode. As reported elsewhere, a change in slope as those shown by OMC + *B. subtilis* and OMC015 + *B. subtilis* compared to OMC and OMC015, respectively, may be ascribed to c-type cytochromes promoting the bioelectrochemical reaction by enhancing the EET via a direct mechanism (Liu, *et al*., 2017). Moreover, as indicated previously, higher j values in the anodic and cathodic scans can be ascribed to improved oxidation reactions and/or faster electron transfer, and to the reduction of accumulated metabolic intermediates, respectively (Modestra & Mohan, 2014).

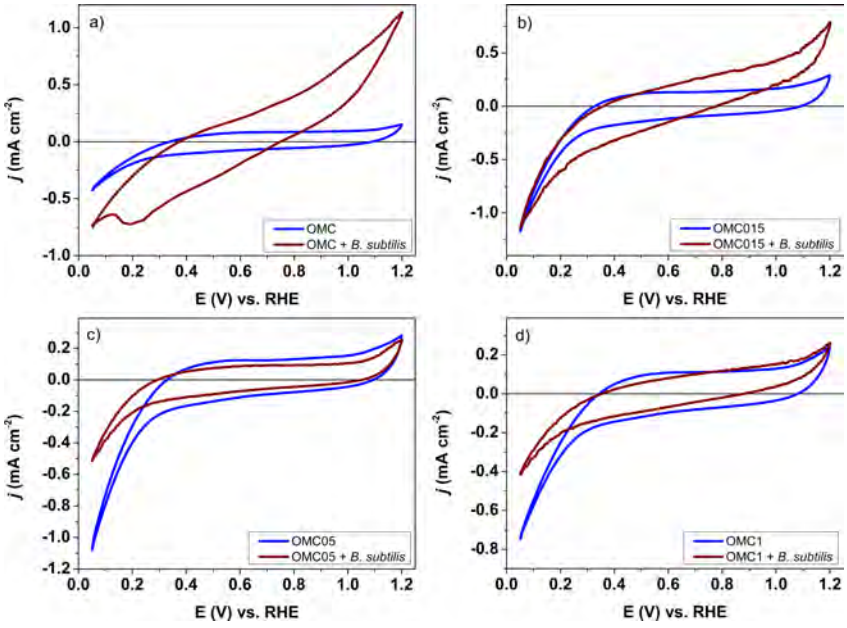

Figure 8. CVs of the bioanodes containing the OMC catalysts + *B. subtilis* and the anodes formed only by the carbon materials in PWW. Scan rate: 20 mV s^{-1}.

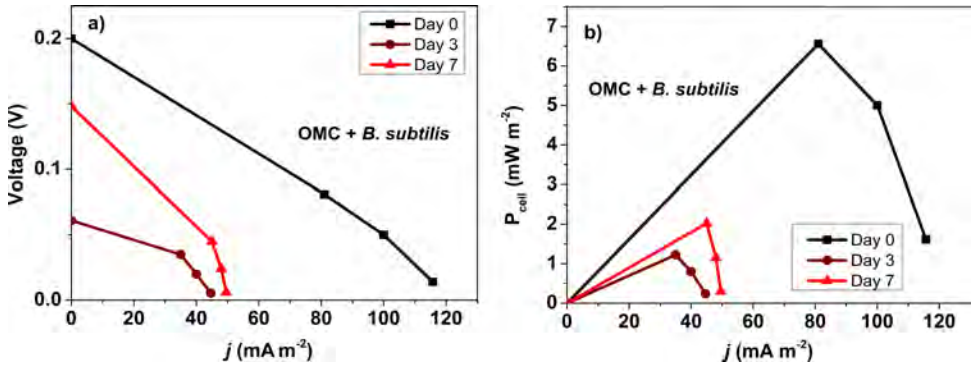

Figure 9. a) V-j and b) P_{cell}-j curves of the MFC equipped with the OMC + *B. subtilis* bioanode at Days 0, 3, and 7. Membrane: Nafion 117. Cathode: Pt/C. Anode substrate: PWW. Cathode electrolyte: O_2-saturated phosphate buffer solution. T_{cell}: ambient.

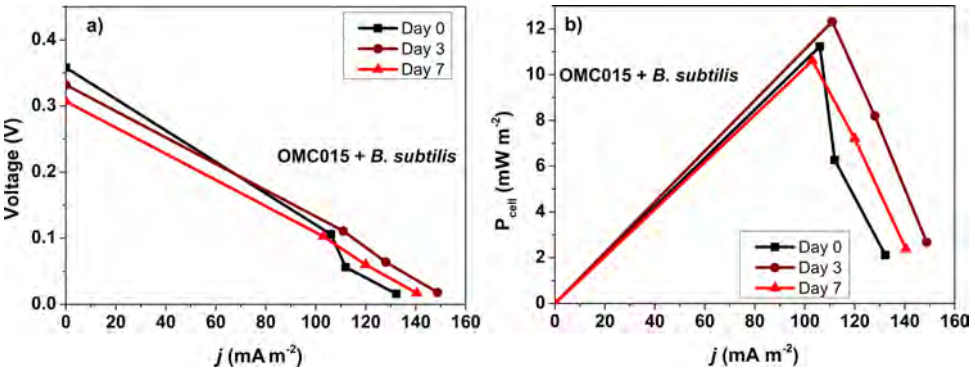

Figure 10. a) V-j and b) P_{cell}-j curves of the MFC equipped with the OMC015 + *B. subtilis* bioanode at Days 0, 3, and 7. Membrane: Nafion 117. Cathode: Pt/C. Substrate: PWW. Cathode electrolyte: O_2-saturated phosphate buffer solution. T_{cell}: ambient.

In the case of the OMC05 + *B. subtilis* and OMC1 + *B. subtilis* bioanodes, their j values become smaller than their anode counterparts (i.e., OMC05 and OMC1, respectively), thus showing a lower bioelectrochemical performance with the microorganisms. Such results demonstrate that, despite the growth of a biofilm (see Figures 7 e-h), the EET between the catalyst layer and biofilm is rather poor at these bioanodes, limiting the oxidation of organic matter from PWW. It is hypothesized that the thickness of the biofilm at these bioanodes is higher than an optimal value expected for a fast EET, becoming rather resistive and resulting in low j values generated with the EAM. Moreover, one factor that may have affected the performance of OMC05 and OMC1 is their lower surface area, compared to OMC and OMC015 (Table 2). Considering this behavior, only the OMC + *B. subtilis* and OMC015 + *B. subtilis* bioanodes have been further evaluated in the full MFC.

Figures 9 a-b) show the polarization and power density curves of the MFC equipped with the OMC + *B. subtilis* bioanode, with PWW as the substrate, at Days 0, 3 and 7 of testing. At Day 0, the OCV is 0.20 V, delivering a maximum j of 115.7 mA m^{-2}, with P_{cell}= 6.56 mW m^{-2} (Tabl3 S3). After 3 days of operation, the overall performance decays drastically in terms of OCV and j, delivering P_{cell}= 1.22 mW m^{-2}. Such decrease in bioelectrochemical activity can be attributed partially to the so-called microbial log phase, at which during a given time lapse the microorganisms utilize the metabolic energy for their extracellular development (Serra, *et al*., 2020; Masoodi, *et al*., 2021), thus there is a clear decrease in P_{cell}.

At Day 7, the OCV increases compared to Day 3, but remains lower than Day 0 (i.e., 0.15 V). The j generated by the MFC at Day 7 is also lower than Day 0, with P_{cell}= 2.02 mW m^{-2} (Table S3), suggesting an adaptation of the microorganism, reaching a stationary phase of its growth, enhancing the electron transfer from the PWW related to Day 3, but not reaching the initial performance of Day 0. The oscillating behavior of the MFC can also be a result of the dynamic features of the OMC + *B. subtilis* bioanode, where the biofilm can be evolving during the operation, probably forming/eliminating other bacteria.

Figures 10 a-b) show the polarization and power density curves of the MFC equipped with the OMC015 + *B. subtilis* bioanode. In this case, the behavior is less oscillating, resulting in a more stable operation of the MFC. For instance, the OCV is 0.35, 0.33, and 0.30 V at Days 0, 3, and 7, respectively. The highest j is 148.8 mA m^{-2} at Day 3, which is relatively like that at Day 7 (Table S3). The maximum P_{cell} is 12.3 mW m^{-2} at Day 3, which is higher than the maximum in Figure 9 b). Opposite to the behavior observed in Figure 9, the performance of the MFC with the OMC015 + *B. subtilis* bioanode in the 7-days test indicates a fast extracellular development of the biofilm formed by the EAM, along with a high biocompatibility between OMC015 and the bacteria, resulting in relatively equal EET from the PWW during the long-term test (Pinto, *et al*., 2018).

Table S4 shows a comparison of P_{cell} values generated by MFCs using *B. subtilis* as the EAM in different substrates. The application of the MFCs is also reported. The P_{cell} of this work compares favorably to those where a substrate other than PWW has been used, except for the wearable application in sweat. As for the PWW as substrate, in the previous works of Table S4 its pH is reported as 9.6, while here it is 7.1. Therefore, there is an important effect of the alkalinity of the substrate on the bioelectrochemical behavior of *B. subtilis*, limiting the generation of energy when it drops to nearly neutral environments.

Figure 11 shows the Nyquist plots of the OMC + *B. subtilis* and OMC015 + *B. subtilis* bioanodes. The fit was performed using a Randles equivalent circuit (inset) to determine the ohmic (R1) and charge transfer resistance of the bioanodes (Rct, identified as R2), the non-ideal capacitive behavior (constant phase element, Q), and the limitations due to diffusion of species (Warburg element, W) (Ramasamy, *et al*., 2008). The R2 values of OMC + *B. subtilis* and OMC015 + *B. subtilis* have been determined as 6730 and 3638 Ω, respectively. Moreover, with the OMC015 + *B. subtilis* bioanode, the linear behavior due to diffusion limitations at low frequencies is more important than that of OMC + *B. subtilis*.

Nevertheless, the results indicate that the Rct decreases when the OMC is functionalized with methanol (OMC015 catalyst), which agrees with the previous reports by our research group (Duarte-Urbina, *et al*., 2021). This lower Rct correlates well with the higher performance of the MFC equipped with the OMC015 + *B. subtilis* bioanode at Day 0 (Figure 10) compared to that with OMC + *B. subtilis* at the same Day (Figure 9) in terms of j and P_{cell}.

A comparison with previous reports shows that bioanodes with modified carbon cloth (CC) using a microalgae-derived nitrogen-rich biocarbon (CCP-CC) have Rct values of 264.7 and 59.3 Ω, respectively (Lan, *et al*., 2020). Elsewhere, the polarization resistance of carbon felt + *S. oneidensis* and carbon felt only electrodes has been reported as 10.2 and 7790 kΩ, respectively (Manohar, *et al*., 2008). The authors report that the Rct is the major contribution to the total internal resistance of the MFC, which is lower for MFC that contained the microbial biofilm. Other workers agree that the Rct values decrease due to the biofilm presence (Ren, *et al*., 2011). In such report, a carbon paper has been implemented as anode material, with an initial Rct of 9 kΩ, which decreases to 2.5 kΩ after two weeks of operation because of the growth of a biofilm on the anode surface.

Although it is a hard task to compare different MFC bioanode systems, the previous reports indicate that the Rct values calculated for the OMC + *B. subtilis* and OMC15 + *B. subtilis* bioanodes are within the range expected for this type of bioelectrochemical devices. Here, it is shown that the functionalization treatment with methanol modifies the structural properties and increases the presence of O-H bonds, which in addition to promoting the biocompatibility between the catalyst and the EAM, has a positive effect reducing the charge transfer resistance. The lower R2 value, along with the fact that OMC015 has the highest specific surface area, can explain why the OMC015 + *B. subtilis* bioanode generates the highest *j* values in the polarization curves with a more stable behavior.

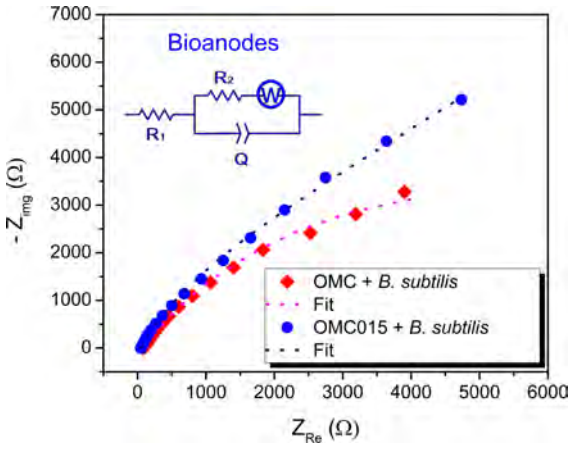

Figure 11. Nyquist plots and Randles equivalent circuit (inset) of the OMC + *B. subtilis* and OMC015 + *B. subtilis* bioanodes evaluated at Day 0 of the MFC testing. Anode substrate: PWW; cathode electrolyte: O_2-saturated phosphate buffer solution.

Conclusions

Surface functionalization of OMC with several concentrations of MeOH resulted in the development of O-H groups. The microwave treatment with 0.15 mol L^{-1} MeOH increased the surface area and total pore volume of OMC015 compared to non-functionalized OMC, ascribed to the removal of impurities, along with the penetration and activation of pores by the diluted solution under intermittent heating. Meanwhile, treatment with 0.5 and 1 mol L^{-1} MeOH decreased both surface area and total pore volume.

Overall, extracellular development of a biofilm by *B. subtilis* was observed at the catalyst layers of OMC, OMC015, OMC05, and OMC1. Nevertheless, CV analysis demonstrated a poor behavior of the OMC05 + *B. subtilis* and OMC05 + *B. subtilis* bioanodes in PWW, ascribed to a thicker biofilm which increases the resistance to electron transfer. The poor performance of such bioanodes may also be related to the low surface area of those carbon catalysts.

In MFC tests, both OMC + *B. subtilis* and OMC015 + *B. subtilis* bioanodes generated bioenergy from the organic matter of PWW. The latter showed a more stable operation at Days 0, 1, and 3 of long-term testing, attributed to a homogeneous extracellular development of the biofilm and a high biocompatibility between the EAM and OMC015. Such biocompatibility was ascribed to the high surface area and the presence of functional groups at OMC015. As a result, the P_{cell} obtained from the MFC with the OMC015 + *B. subtilis* bioanode varied only slightly during evaluation, reaching a maximum value of 12.32 mW m^{-2} at Day 3.

Acknowledgment

To Conacyt and Coecyt for financial support to the projects (CB-241526, CB-250632 and CB-287225, COAH-2019-C13-006, COAH-2019-C13-010, COAH-2021-C15, COAH-2021-C15-C095). SGM thanks Conacyt for PhD scholarship granted and to Cinvestav Unidad Saltillo for

the opportunity and resources provided during her doctoral studies.

References

Al-Ansari, M., Benabdelkamel, H., Al-Humaid, L. (2021). Degradation of sulfadiazine and electricity generation from wastewater using *Bacillus subtilis* EL06 integrated with an open circuit system. *Chemosphere 276*, 130145. doi: 10.1016/j.chemosphere.2021.130145

Al-Gheethi, A., Noman, E., Mohamed, R., Ismail, N., Abdullah, A., Kassim, A. (2019). Optimizing of pharmaceutical active compounds biodegradability in secondary effluents by β-lactamase from *Bacillus subtilis* using central composite design. *Journal of Hazardous Materials 365*, 883-894. doi: 10.1016/j.jhazmat.2018.11.068

Alonso-Lemus, I., Cobos-Reyes, C., Figueroa-Torres, M., Escobar-Morales, B., Aruna, K., Akash, P., Rodríguez-Varela, F.J. (2022). Green power generation by microbial fuel cells using pharmaceutical wastewater as substrate and electroactive biofilms (bacteria/biocarbon). *Journal of Chemistry 2022*, 1963973. doi: 10.1155/2022/1963973

Bharti, A., Cheruvally, G. (2017). Influence of various carbon nano-forms as supports for Pt catalyst on proton exchange membrane fuel cell performance. *Journal of Power Sources 360*, 196-205. doi: 10.1016/j.jpowsour.2017.05.117.

Carrillo-Rodríguez, J., Garay-Tapia, A., Escobar-Morales, B., Escorcia-García, J., Ochoa-Lara, M., Rodríguez-Varela, F.J., Alonso-Lemus, I. (2021). Insight into the performance and stability of N-doped ordered mesoporous carbon hollow spheres for the ORR: Influence of the nitrogen species on their catalytic activity after ADT. *International Journal of Hydrogen Energy 46*, 26087-26100. doi: 10.1016/j.ijhydene.2021.01.047

Conzuelo, F., Ruff, A., Schuhmann, W. (2018). Self-powered bioelectrochemical devices. *Current Opinion in Electrochemistry 12*, 156-163. doi: 10.1016/j.coelec.2018.05.010

Cui, D., Wang, Y., Xing, L., Li, W. (2014). Which determines power generation of microbial fuel cell based on carbon anode, surface morphology or oxygen containing group? *International Journal of Hydrogen Energy 39*, 15081-15087. doi: dx.doi.org/10.1016/j.ijhydene.2014.07.095

Duarte-Urbina, O., Rodríguez-Varela, F.J., Fernández-Luqueño, F., Vargas-Gutiérrez, G., Sánchez-Castro, M., Escobar-Morales, B., Alonso-Lemus, I. (2021). Bioanodes containing catalysts from onion waste and *Bacillus subtilis* for energy generation from pharmaceutical wastewater in a microbial fuel cell. *New Journal of Chemistry 45*, 12634-12646. doi: 10.1039/d1nj01726h

Gang, Y., Li, B., Fang, S., Pellessier, J., Fang, L., Pan, F., Du, Z., Hu, Y.H., Li, T., Wang, G., Li, Y. (2023). Efficient electrochemical CO_2 reduction to CO by metal and nitrogen co-doped carbon catalysts derived from pharmaceutical wastes adsorbed on commercial carbon nanotubes. *Chemical Engineering Journal 453*, 139712. doi: 10.1016/j.cej.2022.139712

García-Mayagoitia, S., Fernández-Luqueño, F., Morales-Acosta, D., Carrillo-Rodríguez, J., García-Lobato, M., De la Torre-Saenz, L., Alonso-Lemus, I.L., Rodríguez-Varela, F.J. (2019). Energy generation from pharmaceutical residual water in microbial fuel cells using ordered mesoporous carbon and *Bacillus subtilis* as bioanode. *ACS Sustainable Chemistry and Engineering 7*, 12179-12187. doi: 10.1021/acssuschemeng.9b01281

He, Z., Mansfeld, F. (2009). Exploring the use of electrochemical impedance spectroscopy (EIS) in microbial fuel cell studies. *Energy & Environmental Science 2*, 215-219. doi: 10.1039/b814914c

International Energy Agency. (2023). *World Energy Balances*. Retrieved May 29th, 2023, from https://www.iea.org/reports/world-energy-balances-overview

Islam, A., Teo, S., Ng, C., Taufiq-Yap, Y., Choong, S., Awal, M. (2023). Progress in recent sustainable materials for greenhouse gas (NO_x and SO_x) emission mitigation. *Progress in Materials Science 132*, (101033). doi: 10.1016/j.pmatsci.2022.101033

Kan, X., Song, F., Zhang, G., Zheng, G., Zhu, Q., Liu, F., Jiang, L. (2023). Sustainable design of co-doped ordered mesoporous carbons as efficient and long-lived catalysts for H_2S reutilization. Chemical Engineering Science 269, (118483). doi: 10.1016/j.ces.2023.118483

Kipf, E., Koch, J., Geiger, B., Erben, J., Richter, K., Gescher, J., Zengerle, R., Kerzenmacher, S. (2013). Systematic screening of carbon-based anode materials for microbial fuel cells with *Shewanella oneidensis* MR1. *Bioresource Technology 146*, 386-392. doi: 10.1016/j.biortech.2013.07.076

Lan, L., Li, J., Feng, Q., Zhang, L., Fu, Q., Zhu, X., Liao, Q. (2020). Enhanced current production of the anode modified by microalgae derived nitrogen-rich biocarbon for microbial fuel cells. *International Journal of Hydrogen Energy 45*, 3833-3839. doi: 10.1016/j.ijhydene.2019.06.199.

Lian, Q., Konggidinata, M., Ahmad, Z., Gang, D., Yao, L., Subramaniam, R., Revellame., Holmes, W.B. Zappi, M. (2019). Combined effects of textural and surface properties of modified ordered mesoporous carbon (OMC) on BTEX adsorption. *Journal of. Hazardous Materials 377*, 381-390. doi: https://doi.org/10.1016/j.jhazmat.2019.05.079

Lilloja, J., Mooste, M., Kibena-Põldsepp, E., Sarapuu, A., Kikas, A., Kisand, V., Käärik, M., Kozlova, J., Treshchalov, A., Paiste, P., Aruväli, J., Leis, J., Tamm., Holdcroft, S., Tammeveski, K. (2023). Cobalt-, iron- and nitrogen-containing ordered mesoporous carbon-based catalysts for

anion-exchange membrane fuel cell cathode. *Electrochimica Acta 439*, (141676). doi: 10.1016/j.electacta.2022.141676

Liu, T., Yu, Y., Chen, T., Chen, W. (2017). A synthetic microbial consortium of shewanella and bacillus for enhanced generation of bioelectricity. *Biotechnology and Bioengineering 114*, 526-532. doi: 10.1002/bit.26094

Ma, X., Yuan, H., Hu, M. (2019). A simple method for synthesis of ordered mesoporous carbon. *Diamond and Related Materials 98*, (107480). doi: 10.1016/j.diamond.2019.107480

Manohar, A., Bretschger, O., Nealson, K., Mansfeld, F. (2008). The use of electrochemical impedance spectroscopy (EIS) in the evaluation of the electrochemical properties of a microbial fuel cell. *Bioelectrochemistry 72*, 149-154. doi: 10.1016/j.bioelechem.2008.01.004

Masoodi, K., Lone, S., Rasool, R. (2021). Growth of bacterial cultures and preparation of growth curve. In K. Masoodi, S. Lone, R. Rasool, *Advanced Methods in Molecular Biology and Biotechnology* (pp. 163-166). Academic Press. doi: 10.1016/B978-0-12-824449-4.00030-X

Maziarka, P., Wurzer, C., Arauzo, P., Dieguez-Alonso, A., Masek, O., Ronsse, F. (2021). Do you BET on routine? The reliability of N_2 physisorption for the quantitative assessment of biochar's surface area. *Chemical Engineering Journal 418*, (129234). doi: 10.1016/j.cej.2021.129234

Menéndez, J., Arenillas, A., Fidalgo, B., Fernández , Y., Zubizarreta, L., Calvo, E., Bermúdez, J. (2010). Microwave heating processes involving carbon materials. *Fuel Processing Technology 91*, 1-8. doi: 10.1016/j.fuproc.2009.08.021

Modestra, J., Mohan, S. (2014). Bio-electrocatalyzed electron efflux in Gram positive and Gram negative bacteria: an insight into disparity in electron transfer kinetics. *RSC Advances 4*, 34045-34055. doi: 10.1039/c4ra03489a

Morales-Acosta, D., Rodríguez-Varela, F.J., Benavides, R. (2016). Template-free synthesis of OMC: Application as a support of highly active Pt nanoparticles for the oxidation of organic fuels. *International Journal of Hydrogen Energy 41*, 3387-3398. doi: 10.1016/j.ijhydene.2015.10.114

Obata, O., Greenman, J., Kurt, H., Chandran, K., Ieropoulos, I. (2020). Resilience and limitations of MFC anodic community when exposed to antibacterial agents. *Bioelectrochemistry 134*, (107500). doi: doi.org/10.1016/j.bioelechem.2020.107500

Pant, D., Patil, S. (2022). Microbially catalyzed bioelectrochemical power devices come of age. *Joule 6*, 1399-1401. doi: 10.1016/j.joule.2022.06.033

Patel , N., Rai, D., Chauhan, D., Mishra, U., Bhunia, B. (2019). Carbon nanotube based anodes and cathodes for microbial fuel cells. In: *Microbial Fuel Cells: Materials and Applications*, (Inamuddin, M. Faraz-Ahmer, A. Asiri, eds.), pp. 125-150. Materials Research Forum LLC. doi: 10.21741/9781644900116-6

Pérez-Rodríguez, S., Sebastián, D., Lázaro, M. (2019). Electrochemical oxidation of ordered mesoporous carbons and the influence of graphitization. *Electrochimica Acta 303*, 167-175. doi: 10.1016/j.electacta.2019.02.065

Pinto, D., Coradin, T., Laberty-Robert, C. (2018). Effect of anode polarization on biofilm formation and electron transfer in Shewanella oneidensis/graphite fuel microbial fuel cells. *Bioelectrochemistry 120*, 1-9. doi: 10.1016/j.bioelechem.2017.10.008

Plekhanova, Y., Rai, M., Reshetilov, A. (2022). Nanomaterials in bioelectrochemical devices: on applications enhancing their positive effect. *3 Biotech 12*, 231. doi: 10.1007/s13205-022-03260-w

Ramasamy, R., Ren, Z., Mench, M., Regan, J. (2008). Impact of initial biofilm growth on the anode impedance of microbial fuel cells. *Biotechnology and Bioengineering 101*, 101-108. doi: 10.1002/bit.21878

Rashid, T., Sher, F., Hazafa, A., Hashmi, R., Zafar, A., Rasheed, T., Hussain, S. (2021). Design and feasibility study of novel paraboloid graphite based microbial fuel cell for bioelectrogenesis and pharmaceutical wastewater treatment. *Journal of Environmental Chemical Engineering 9*, 104502. doi: 10.1016/j.jece.2020.104502

Ren, Z., Ramasamy, R., Cloud-Owen, S., Yan, H., Mench, M., Regan, J. (2011). Time-course correlation of biofilm properties and electrochemical performance in single-chamber microbial fuel cells. *Bioresource Technology 102*, 416-421. doi: 10.1016/j.biortech.2010.06.003

Rodríguez-Varela, F.J., Savadogo, O. (2009). Ethanol-tolerant Pt-alloy cathodes for direct ethanol fuel cell (DEFC) applications. *Asia-Pacific Journal of Chemical Engeneering 4*, 17-24. doi: 10.1002/apj.193

Ryu, J., Landers, M., Choi, S. (2022). A sweat-activated, wearable microbial fuel cell for long-term, on-demand power generation. *Biosensors and Bioelectronics 205*, 114128. doi: 10.1016/j.bios.2022.114128

Serra, P., Espíritu-Santo, A., Magrinho, M. (2020). A steady-state elecrical model of a microbial fuel cell through multiple-cycle polarization curves. *Renewable and Sustainable Energy Reviews 117*, 109439. doi: 10.1016/j.rser.2019.109439

Szopińska, M., Ryl, J., Pierpaoli, M. (2023). Closing the loop: Upcycling secondary waste materials into nanoarchitectured carbon composites for the electrochemical degradation of pharmaceuticals. *Chemosphere 313*, 137631. doi: 10.1016/j.chemosphere.2022.137631

Thommes, M., Kaneko, K., Neimark, A., Olivier, J., Rodríguez-Reinoso, F., Rouquerol, J., Sing, K.

(2015). Physisorption of gases, with special reference to the evaluation of surface area and pore size distribution (IUPAC Technical Report). *Pure and Applied Chemistry 87*, 1051-1069. doi: 10.1515/pac-2014-1117

Vidal, J., Huilinir, C., Santander, R., Silva-Agredo, J., Torres-Palma, R., Salazar, R. (2019). Degradation of ampicilin antibiotic by electrochemical processes: Evaluation of antimicrobial activity of treated water. *Environmental Science and Pollution Research 26*, 4404-4414. doi: 10.1007/s11356-018-2234-5

Wan, X., Li, Y., Xiao, H., Pan, Y., Liu, J. (2020). Hydrothermal synthesis of nitrogen-doped oredered mesorporous carbon via lysine-assisted self-assembly for efficient CO_2 capture. *RSC Advances 10*, 2932-2941. doi: 10.1039/c9ra09983b

Wang, X., Lin, Q., Pan, H., Jia, S., Wu, H., Shi, Y., Wang, Z. (2020). Oxidation modification of chitosan-based mesoporous carbon by soft template method and the adsorption and release properties of hydroxycamptoecin. *Scientific Reports 10*, 15772. doi: 10.1038/s41598-020-72933-4

Weidenthaler, C., Lu, A., Schmidt, W., Schüth, F. (2006). X-ray photoelectron spectroscopic studies of PAN-based ordered mesoporous carbons (OMC). *Microporous Mesoporous Materials 88*, 238-243. doi: 10.1016/j.micromeso.2005.09.015

Xiao, N., Wu, R., Huang, J., Selvaganapathy, P. (2020). Anode surface modifications regulates biofilm community population and the performance of micro-MFC based biochemical oxygen demand sensor. *Chemical Engineering Science 221*, 11569. doi: 10.1016/j.ces.2020.115691

Zhang, J., Zhou, Y., Yao, B., Yang, J., Zhi, D. (2021). Current progress in electrochemical anodic-oxidation of pharmaceuticals: Mechanisms, influencing factors, and new technique. *Journal of Hazardous Materials 418*, 126313. doi: 10.1016/j.jhazmat.2021.126313

Zhao, P., Zhang, H., Sun, X., Hao, S., Dong, S. (2022). A hybrid bioelectrochemical device based on glucose/O_2 enzymatic biofuel cell for energy conversion and storage. *Electrochimica Acta 420*, 140440. doi: 10.1016/j.electacta.2022.140440

Zhou, M., Yang, J., Wang, H., Jin, T., Hassett, D., Gu, T. (2014). Bioelectrochemistry of Mirobial Fuel Cell and their Potential Applications in Bioenergy. In *Bioenergy Reearch: Advances and Applications*, (V.K. Gupta, M.G. Tuohy, C.P. Kubicek, J. Saddler, F. Xu, eds.), pp. 132-147. Elsevier, New York. doi: 10.1016/B978-0-444-59561-4.00009-7